Membrane Topology of the β-Subunit of the Oxaloacetate Decarboxylase Na^+ Pump from *Klebsiella pneumoniae*†

Petra Jockel, Marco Di Berardino, and Peter Dimroth*

Mikrobiologisches Institut der Eidgenössischen Technischen Hochschule, ETH-Zentrum, CH-8092 Zürich, Switzerland

Received February 9, 1999; Revised Manuscript Received June 7, 1999

ABSTRACT: The topology of the β-subunit of the oxaloacetate Na^+ pump (OadB) was probed with the alkaline phosphatase (PhoA) and β-galactosidase (lacZ) fusion technique. Additional evidence for the topology was derived from amino acid alignments and comparative hydropathy profiles of OadB with related proteins. Consistent results were obtained for the three N-terminal and the six C-terminal membrane-spanning α-helices. However, the two additional helices that were predicted by hydropathy analyses between the N-terminal and C-terminal blocks did not conform with the fusion results. The analyses were therefore extended by probing the sideness of various engineered cysteine residues with the membrane-impermeant reagent 4-acetamido-4′-maleimidylstilbene-2,2′-disulfonate. The results were in accord with those of the fusion analyses, suggesting that the protein folds within the membrane by a block of three N-terminal transmembrane segments and another one with six C-terminal transmembrane segments. The mainly hydrophobic connecting segment is predicted not to traverse the membrane fully, but to insert in an undefined manner from the periplasmic face. According to our model, the N-terminus is at the cytoplasmic face and the C-terminus is at the periplasmic face of the membrane.

Oxaloacetate decarboxylase of *Klebsiella pneumoniae*, whose overall geometry and function are shown in Figure 1, consists of three different subunits, α, β, and γ with molecular masses of 63.5, 44.9, and 8.9 kDa, respectively (*1*−*5*). The cytoplasmic biotin-containing α-subunit is bound to the membrane-embedded β- and γ-subunits, which were shown to be closely associated (*6*−*8*). The catalytic reaction cycle starts with the carboxyl transfer from oxaloacetate to the prosthetic biotin group that is attached to the C-terminal part of the α-subunit. This reaction is catalyzed at a low rate by the α-subunit alone (*7*). In the additional presence of the Zn^{2+}-containing γ-subunit, the rate increases approximately 1000-fold, probably because the metal ion polarizes the carbonyl oxygen bond of oxaloacetate, thereby facilitating the carboxyl transfer to biotin (*6*). The carboxybiotin now moves from the carboxyl transfer site at the α-subunit to the decarboxylase site at the β-subunit. The mobility of the biotin residue is facilitated by an extended alanine/proline linker in the interdomain region between the carboxyltransferase and the biotin domain (*3*). During the course of the subsequent decarboxylation reaction, one to two Na^+ ions are pumped across the membrane into the periplasm, and one H^+ traverses the membrane in the opposite direction. This proton is consumed during the release of CO_2 from the biotin carboxylate (*7*, *9*).

The *oadGAB* genes encoding the γ-, α-, and β-subunits of oxaloacetate decarboxylase have been cloned, sequenced, and functionally expressed in *Escherichia coli* (*1*−*3*, *6*). These genes are clustered on the chromosome together with other genes of the fermentative citrate metabolism (*10*).

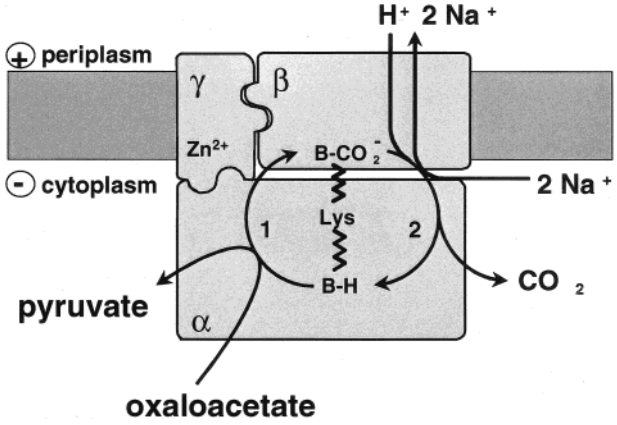

FIGURE 1: Cartoon showing the overall geometry and features of the catalytic events: B-H, biotin; B-CO_2^-, carboxybiotin; Lys, biotin-binding residue; 1, carboxyltransferase reaction; and 2, decarboxylase reaction. For details, see the text.

Previous experiments already demonstrated that the β-subunit (OadB) is specifically protected by Na^+ ions from proteolytic digestion, suggesting a Na^+ binding site on this protein (*7*, *11*). Complementary evidence for the presence of a Na^+ binding site on the β-subunit has been obtained with the related Na^+ pumps glutaconyl-CoA decarboxylase (*12*) and methylmalonyl-CoA decarboxylase (*13*). Conspicuous residues for such a site are two conserved aspartate residues (D149 and D203) within hydrophobic domains of the β-subunit. While mutagenesis of D149 to E or N did not yield a new phenotype, mutants with a D203E or D203N substitution were completely inactive, not only in Na^+ transport but also in the decarboxylation of oxaloacetate, whereas the carboxyltransferase activity was retained (*9*). On the basis of these and other results, a direct coupling

† This work was supported by the Swiss National Science Foundation.

* To whom correspondence should be addressed. Telephone: 0041 1 632 33 21. Fax: 0041 1 632 13 78. E-mail: dimroth@micro.biol.ethz.ch.

10.1021/bi990303+ CCC: $18.00
Published on Web 09/24/1999

mechanism has been proposed, in which D203 plays an essential role in both the vectorial and the chemical reaction. In the proposed mechanism, the carboxybiotin binds together with a Na^+ ion close to D203 of the β-subunit. Subsequently, the Na^+ ion is envisaged to switch to D203, and simultaneously, the proton originally bound to this residue moves to the biotin carboxylate, where it catalyzes immediate decarboxylation of this acid-labile compound. This exergonic reaction is coupled to the release of the bound Na^+ ion to the positive side of the membrane (*9*).

To select further amino acids for mutational analyses, we have investigated the topology of OadB by gene fusion analyses and by determining the sideness of several engineered cysteine residues with a membrane-impermeable probe. The results indicate a topology for OadB, consisting of nine transmembrane helices with interconnecting cytoplasmic and periplasmic loops. Interestingly, a hydrophobic and highly conserved domain (segment IIIa, Figure 6B), linking helices III and IV that includes the catalytically essential D203 residue, does not appear to fold into membrane-spanning α-helices, as suggested from hydrophobic profiles. Part of this region rather seems to be oriented to the outer surface of the membrane, while other parts reside within the membrane but do not penetrate through it. On the basis of these results, a new topology model for OadB is proposed. Numbering of the hydrophobic segments and the connecting loops in the following text is based on this model (Figure 6B).

EXPERIMENTAL PROCEDURES

Bacterial Strains

The bacterial strains used in this study are *E. coli* DH5α (Bethesda Research Laboratories, Bethesda, MD), *E. coli* JM110 (*14*), and *E. coli* CC118 (*15*).

Media and Reagents

The screening of active alkaline phosphatase (AP)[1] and β-galactosidase fusion proteins was performed on Luria Bertani (LB) plates containing 100 μg/mL ampicillin, 40 μg/mL 5-bromo-4-chloro-3-indolyl phosphate, or 40 μg/mL 5-bromo-3-indolyl β-D-galactopyranoside and 1 mM isopropyl β-D-thiogalactopyranoside (IPTG).

Recombinant DNA Techniques

Standard recombinant DNA techniques were performed essentially as described by Sambrook et al. (*16*). Polymerase chain reactions (PCRs) were performed using Vent Polymerase from New England Biolabs (Beverly, MA). DNA sequencing was carried out according to the dideoxynucleotide chain termination method (*17*) using a *Taq* DyeDeoxy terminator cycle sequencing kit and the ABI Prism 310 genetic analyzer from Applied Biosystems.

Construction of oadB−'phoA Gene Fusions

Nested Deletions of the oadB Gene from Its C-Terminus. The '*phoA* gene lacking its leader sequence was removed as a *Pst*I−*Nla*IV fragment from pCH2 (*18*) and cloned into pKAB (downstream of the β-subunit), which was digested with the compatible enzymes *Nsi*I and *Nru*I, resulting in plasmid pKAB-'PhoA. pKAB was constructed by replacing the *Bcl*I−*Sac*I fragment of pSK-BXY (*6*) with the corresponding fragment obtained with PCR techniques, using primer A (5′-ACGCGC**TGATCA**ACATCGTC-3′) on the *Bcl*I site (bold letters) of the β-subunit and primer KAB-fus (5′-cgat*cccggg***tcgcga**tagatgcat*gagctc*a**gcggccgC**-TACATCGCCAGCACGTACT-3′) at the C-terminus of the β-subunit (uppercase letters represent complementary bases at the C-terminus; the bases depicted in lowercase letters introduced the following restriction sites: *Sma*I in italics, *Nru*I in bold, *Nsi*I underlined, *Sac*I underlined in italics, and *Not*I underlined in bold). Exonuclease III was used to progressively digest *oadB* from its 3′-end via the 5′-overhang created by *Not*I digestion of pKAB-'PhoA, essentially according to the method of Henikoff (*19*). The '*phoA* gene was protected from exonuclease III digestion by the 3′-overhang-generating *Sac*I site. After treatment with S1 nuclease and Klenow fragment, the ends were ligated together and the resulting plasmids transformed into competent *E. coli* CC118 cells. The screening of in-frame fusions was performed on LB plates, containing 5-bromo-4-chloro-3-indolyl phosphate, IPTG, and ampicillin (100 μg/mL). Plasmid DNA of blue and pale blue colonies was further examined by restriction analysis to approximately localize the fusion site and subjected to sequence analysis.

Site-Directed phoA Fusions to Predicted Cytoplasmic and Periplasmic Loops of the β-Subunit. The primers used for the synthesis of PCR products, containing the N-terminal region of *oadB*, to which the '*phoA* gene had to be fused and the resulting fusion sites are listed in Table A of the Supporting Information. Fusions to the predicted periplasmic loop 4 (E217) as well as to putative cytoplasmic loops 2 (V80 and G134), 5 (L257), 7 (Q338), and 9 (A398) were obtained as follows. The PCR product resulting from primer B_{NH2} and the corresponding primer for a specific fusion site (L1, -4, -5, and -8; see the Supporting Information) was digested with *Kpn*I and used to replace the *oadB*-containing *Kpn*I−*Sac*I fragment from pKAB-'PhoA. To obtain an in-frame fusion, pKAB-'PhoA was first linearized with *Sac*I, mung bean nuclease treated to remove the 3′-protruding termini, and digested with *Kpn*I. The resulting plasmids were transformed into CC118 cells to determine their phosphatase activity. Further *oadB*−'*phoA*-fusions were constructed by amplifying PCR products from pKAB, using primer B_{NH2} for the N-terminal sequence of *oadB* and primers prP41, prP57, prV80, prP103, prN156, prT179, prG184, prT189, prT245, prL329, and prN365 which define the phoA fusion site. The PCR products were digested with *Kpn*I and *Sac*I and cloned into pKAB-'PhoA, from which the *oadB*-containing *Kpn*I−*Sac*I fragment was removed. For the localization of the C-terminus of the β-subunit, an in-frame PhoA fusion to the C-terminal Met433 was constructed. For this purpose, the PCR product, obtained with primer A and primer PhoA-C_{term} (see the Supporting Information) using pKS-BXY (*6*) as template DNA, was digested with *Bcl*I and *Nru*I and moved into pKAB, replacing the corresponding fragment to yield pKAB2. The *Pst*I−*Nla*IV fragment of pCH2 containing '*phoA* was cloned into pKAB2, which was digested with *Nsi*I and *Nru*I (*Nsi*I and *Pst*I produce compat-

[1] Abbreviations: AP, alkaline phosphatase; IASD, 4-acetamido-4′-maleimidylstilbene-2,2′-disulfonic acid, disodium salt; IPTG, isopropyl β-D-thiogalactopyranoside; LacZ, β-galactosidase; LB, Luria Bertani; MTSET, [2-(trimethylammonium)ethyl]methanethiosulfonate bromide; PhoA, alkaline phosphatase; SDS−PAGE, sodium dodecyl sulfate−polyacrylamide gel electrophoresis; TM, transmembrane.

ible ends), yielding pKAB-PhoA$_{end}$. To make sure that no mutation occurred during the amplification and cloning steps, all PCR products as well as the fusion sites were sequenced.

Construction of oadB−'lacZ Fusions

Site-Directed lacZ Fusions to Predicted Cytoplasmic Loops and the C-Terminus of the β-Subunit. The primers used for the synthesis of PCR products containing the N-terminal region of *oadB* to which the *'lacZ* gene had to be fused and the resulting fusion sites are listed in Table A of the Supporting Information. Fusions to predicted cytoplasmic loop 2 (H72 and V80) and to hydrophobic segment IIIa (Q167, L180, G184, and T189) and to the C-terminus were obtained as follows. The *oadB−'lacZ* fusions were constructed by amplifying PCR products from pKAB, using primer B$_{NH2}$ for the N-terminal sequence of *oadB* and primers prH72lac, prV80lac, prQ167lac, prL180lac, prG184lac, and prT189lac, which define the lacZ fusion site. The PCR products were digested with *Kpn*I and *Apa*I and cloned into pKAB-'lacZ, from which the oadB-containing *Kpn*I−*Not*I fragment had been removed. pKAB-'lacZ was constructed by removing the *'lacZ* gene as a *Dra*I−*Pst*I fragment from pNM480 (*20*) and cloned into pKAB (downstream of the β-subunit), which was digested with the compatible enzymes *Nsi*I and *Nru*I. For the localization of the C-terminus of the β-subunit, an additional in-frame LacZ fusion to the C-terminal Met433 was constructed. For this purpose, the PCR product, obtained with primer A and primer PhoA-C$_{term}$ (see the Supporting Information) using pKS-BXY (*6*) as template DNA, was digested with *Bcl*I and *Nru*I and moved into pKAB, replacing the corresponding fragment to yield pKAB2. The *Pst*I−*Dra*I fragment of pNM 481 (*20*), containing *'lacZ*, was cloned into pKAB2, which was digested with *Nsi*I and *Nru*I (*Nsi*I and *Pst*I produce compatible ends), yielding pKAB-LacZ$_{end}$. To make sure that no mutation occurred during the amplification and cloning steps, all PCR products as well as the fusion sites were sequenced.

Site-Directed Cysteine Mutants of the β-Subunit

The primers used for the site-directed mutagenesis are listed in Table B of the Supporting Information. Site-directed cysteine mutants, placed into predicted cytoplasmic loop 2 and into hydrophobic segment IIIa, were obtained as follows. The PCR fragments, containing the mutation, were constructed with a two-step protocol. For the N-terminal part of the PCR fragments of the β-subunit, primer prN and primers prV129Crev, prL178Crev, prY182Crev, prS187Crev, prP191Crev, prA194Crev, prI198Crev, and prP205Crev were used; pSK-GABC87A served as the template. For the corresponding PCR fragments for the C-terminal part of the β-subunit, primer prC and primers prV129Cfor, prL178Cfor, prY182Cfor, prS187Cfor, prP191Cfor, prA194Cfor, prI198Cfor, and prP205Cfor were used; pSK-GABC87A served as the template. After purification, those PCR fragments served as templates to yield the PCR products from primers prN and prC. The PCR products from this second step contained the mutation. PCR fragments were digested with *Kpn*2I and *Bcl*I and cloned into pSK-GAB (*6*). From pSK-GAB, which was isolated from JM110 cells, the *Kpn*2I−*Bcl*I fragment was removed. Site-directed cysteine mutants, placed into the N- and C-termini, were obtained as follows. The PCR fragments, containing the mutation, were constructed with a two-step protocol, as mentioned above. For the mutation at the N-terminus of the β-subunit, primers prNruIfor and prL7Crev were used for the N-terminal part of the PCR fragment. For the C-terminal part of the PCR fragment, primers prNrev and prL7Cfor were used. Plasmid pSK-GAB served as the template. After purification, those PCR fragments served as templates to yield the PCR products from primers prNruIfor and prNrev. For the mutation at the C-terminus of the β-subunit, primers prBN and prV430Crev were used for the N-terminal part of the PCR fragment and primers prBC and prV430Cfor were used for the C-terminal part. Plasmid pSK-GAB served as the template. After purification, those PCR fragments served as templates to yield the PCR products from primers prBN and prBC. The PCR products from this second step contained the mutation. PCR fragments were digested with *Nru*I and *Kpn*2I (L7C mutation) or *Bcl*I and *Bst*1107I (V430C mutation) and cloned into pSK-GABC87A. From pSK-GABC87A, which was isolated from *E. coli* JM110 cells, the *Nru*I−*Kpn*2I (L7C mutation) or *Bcl*I−*Bst*1107I (V430C mutation) fragment was removed. Plasmid pSK-GABC87A was obtained the same way, using primers prC87Arev and prC87Afor, and prN and prC, with pSK-GAB (*6*) as the template.

Enzyme Assays

Assays of Alkaline Phosphatase and β-Galactosidase Activities. Precultures of *E. coli* CC118 cells harboring the *oadB−'phoA* fusion plasmids were grown overnight in LB medium containing 100 μg/mL ampicillin and used to inoculate 5 mL LB cultures, containing 100 μg/mL ampicillin and 10 mM IPTG. Cultures were grown for 2 h until an A_{600} of 0.5−0.8 was reached. The cells were centrifuged, resuspended in 1 M Tris-HCl (pH 8.0), and washed twice. The cells were resuspended in 3 mL of 1 M Tris-HCl (pH 8.0) to obtain an A_{600} of 0.8−1.0, permeabilized with sodium dodecyl sulfate (SDS) and methylene chloride, and assayed for alkaline phosphatase activity, as described by Miller (*21*) and Pourcher et al. (*22*). Each assay was performed at 37 °C in duplicate on two separate occasions. The units of enzyme activity were calculated according to the references mentioned above. Assays of β-galactosidase activity were perfomed as described by Miller (*21*). Each assay was performed in duplicate on separate occasions. Oxaloacetate decarboxylase activities of site-directed cysteine mutants were determined as described in ref *23*.

Verification of the Expression of the β-Subunit

To be sure that the β-subunit was functionally expressed from the plasmids, which were used as targets for the *'phoA* and *'lacZ* fusion constructs, *E. coli* cells carrying pKS-BXY (*6*), as well as pKAB and pKAB2, were assayed for their ability to reconstitute the decarboxylation activity after incubation with the missing γ- and α-subunits. For this purpose, membrane vesicles of the mentioned *E. coli* clones were prepared, solubilized with 2% Triton X-100, and incubated with isolated γα-complexes as described previously (*6*). The decarboxylation activity was subsequently determined (*23*).

Western Immunoblotting Analysis

Cultures were grown under the same conditions described for the phosphatase assay and β-galactosidase assay experi-

ments and adjusted to an A_{600} of 0.8−1.0. The sedimented cells were resuspended in SDS−PAGE loading buffer, boiled for 5 min, and electrophoresed on 8% (PhoA fusions) and 10% (LacZ fusions) SDS−polyacrylamide gels, according to Schägger and von Jagow (*24*). The proteins were blotted onto a nitrocellulose membrane (Amersham Life Science, Buckinghamshire, U.K.), which was subsequently incubated with antiserum against bacterial alkaline phosphatase or β-galactosidase. Bound antibody was visualized with goat anti-rabbit IgG (PhoA fusions) or goat anti-mouse IgG (LacZ fusions) fused to alkaline phosphatase (AP) (Bio-Rad Laboratories, Richmond, CA, and Sigma-Aldrich) and using nitrotetrazolium blue and 5-bromo-4-chloro-3-indolyl phosphate for color development.

Computer Analyses

Hydropathy plots were created with the TMpred server of the bioinformatics group of the ISREC (Swiss Institute for Cancer Research) (*25*).

Thiol-Specific Fluorescence Labeling

Site-specific fluorescence labeling was designed to selectively alkylate cysteines exposed either to the periplasmic or to the cytoplasmic face of the membrane (*26*). To label cysteines exposed to the periplasm, intact cells (5−6 g wet weight) were harvested by centrifugation (4000*g* for 30 min) and resuspended in 200 mL of buffer A [100 mM sodium sulfate and 50 mM potassium phosphate (pH 8.0)], containing 40 μM freshly prepared IASD. After incubation for 20 min at 23 °C, the labeling reaction was quenched by addition of 2 mM β-mercaptoethanol, followed immediately by three cycles of centrifugation and washing, using buffer A alone. Labeled cells were resuspended in 10 mL of 20 mM potassium phosphate (pH 7.5), 0.5 M NaCl, 1 mM magnesium ethylenediaminetetraacetic acid, 0.02 mM diisopropyl fluorophosphate, and DNase I. Oxaloacetate decarboxylase was purified by affintiy chromatography of a solubilized membrane extract on a SoftLink monomeric avidin−Sepharose column (Promega), as described previously (*23*). The eluate of the avidin−Sepharose column was concentrated in a Biomax 10K centrifugal filter (Millipore) to 50−60 μL.

Cysteines exposed to the cytoplasm were identified with a two-step protocol. External cysteines were blocked by an initial 5 min preincubation of intact cells (5−6 g wet weight) in 200 mL of buffer A, containing 200 μM MTSET (freshly dissolved), a nonfluorescent, membrane-impermeable thiol specific reagent. Excess MTSET was removed by three cycles of centrifugation and washing with buffer A. Cells were resuspended in 10 mL of 20 mM potassium phoshate (pH 7.5), 0.5 M NaCl, 1 mM magnesium ethylenediaminetetraacetic acid, 0.02 mM diisopropyl fluorophosphate, and DNase I. After inside-out vesicles were prepared (*23*), they were dissolved in buffer C [20 mM sodium phosphate (pH 8.0)]. The exposed unmodified cysteines, which had faced the cytoplasm, were labeled by adding 40 μM IASD (freshly dissolved) and incubated for 20 min at 23 °C. The reaction was quenched with 2 mM β-mercaptoethanol, followed immediately by one cycle of centrifugation and washing with buffer C alone. Vesicles were resuspended in 20 mM potassium phosphate (pH 7.5) containing 0.5 M NaCl. Oxaloacetate decarboxylase was purified, as described above, and subjected to SDS−PAGE (20 μg protein per sample, 6.8 μg of βC87A/L7C variant protein per sample), using 10% SDS−polyacrylamide gels according to the method of Schägger and von Jagow (*24*). After electrophoresis, the gel was rinsed briefly with a destaining solution (10% glacial acetic acid/15% methanol), and fluorescence was monitored at an excitation wavelength of 312 nm. The gels were subsequently stained with silver.

RESULTS

Hydropathy Profile and Sequence Alignments of the K. pneumoniae Oxaloacetate Decarboxylase β-Subunit (OadB) with Related Proteins. On the basis of hydropathy plots, a topology for OadB with nine membrane-spanning α-helical segments was proposed previously (*27*). Nine to eleven membrane-spanning α-helices were envisaged for the related β-subunits of the methylmalonyl-CoA decarboxylase (MmdB) Na^+ pumps from *Veillonella parvula* (*28*) and *Propionigenium modestum* (*29*), for the glutaconyl-CoA decarboxylase from *Acidaminococcus fermentans* (*12*), and for the malonate decarboxylase from *Malonomonas rubra* (MadB) (*30*). Additional members of this family have been identified in genome sequencing projects: a MadB homologue in *Rhodobacter capsulatus* and OadB homologues in *Archaeoglobus fulgidus* (*31*) and *Treponema pallidum* (*32*). Hydropathy profiles of a selection of related proteins are shown in Figure 2. Clearly, the profiles reveal a considerable degree of similarity. Characteristic is a very hydrophilic region near the middle of the molecules that is flanked on both sides by a number of hydrophobic stretches. These are mostly connected by only short hydrophilic loops. Ten hydrophobic portions are found in all proteins and have been numbered I, II, III, IIIa, IV, V, VI, VII, VIII, and IX. The most clearly defined hydrophobic stretches in OadB and MmdB are segments I, III−VII, and IX. These are regions predicted to be membrane-spanning domains in previous models (*27*, *28*). The profile of MadB shows that stretch II is clearly an additional hydrophobic domain that must be considered a membrane-spanning α-helical segment. The less pronounced hydrophobicity that is apparent for OadB and MmdB in this region is due to the presence of either glutamate or arginine in these sequences (Figure 3). The other region that might be forming a membrane integral domain of these proteins is area VIII. Due to a conserved arginine or lysine residue in this segment, the hydrophobicity is not very pronounced, and with the profile alone, one cannot predict whether area IX spans the membrane.

The alignment of the sequences of the related proteins, shown in Figure 3, provides additional information about the putative membrane-spanning domains. The most similar regions of these proteins fall into the 10 hydrophobic stretches. Next to segment IIIa, which contains the catalytically essential aspartic acid residue (*9*), the most highly conserved portion is segment VIII. One should notice that the length of nine of the hydrophobic areas of the proteins is conserved, comprising between 20 and 28 amino acid residues, which is in the range expected for membrane-spanning α-helices. Hydrophobic segment IIIa, however, is much longer, which may be due to unusual folding (see below). Gaps of more than one residue can be noticed in the N- and C-terminal portions and in the segment connecting

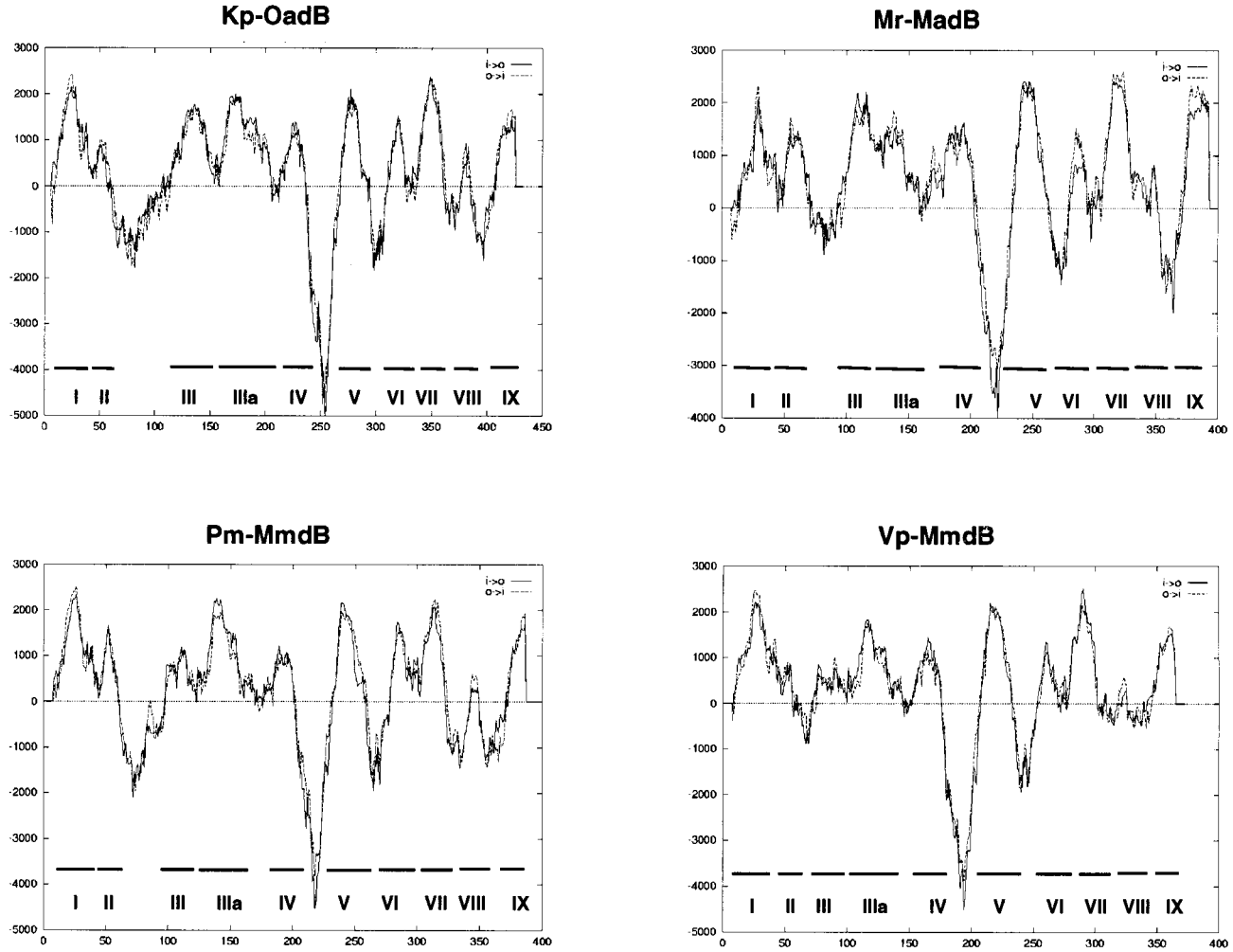

FIGURE 2: Comparative hydropathy plots of the β-subunit of oxaloacetate decarboxylase from *K. pneumoniae* (Kp-OadB) and the related membrane subunits of the Na^+-pumping malonate decarboxylase from *M. rubra* (Mr-MadB) and the methylmalonyl-CoA decarboxylases from *P. modestum* (Pm-MmdB) and *V. parvula* (Vp-MmdB): (—) predicted outside-to-inside helices with the program TMpred (ISREC) and (- - -) predicted inside-to-outside helices with the program TMpred (ISREC).

hydrophobic domains II and III and hydrophobic segment IIIa.

From all these results, the structure of OadB and the related proteins could include 10 transmembrane helical segments. However, no information about the orientation of the protein within the membrane is available from these data. To fill this gap and to become more confident in the predicted membrane topology of OadB, the gene fusion technology with alkaline phosphatase and β-galactosidase was applied (*33*−*36*).

Generation of oadB−*'phoA and oadB*−*'lacZ Gene Fusions.* Two different approaches were used to fuse OadB, truncated to various degrees from the C-terminus, to alkaline phosphatase (AP). One set of fusions was obtained by the nested deletion method with exonuclease III (*19*, *37*), using plasmid pKAB-'PhoA. Gene fusions, encoding hybrid proteins with the decreasing length of OadB at its C-terminus joined to AP, were thus generated. Clones with positive AP activities (transformants of various blue color intensities on XP plates) were selected and subjected to restriction and sequence analyses, as described in Experimental Procedures. In the second approach, PCR technology was applied to cover those areas of the protein within the predicted loop structures and at the C-terminal end that were not already obtained by the first method. Thus, a total of 24 different uniformly distributed OadB−PhoA fusions were obtained by the two different approaches and used for the determination of AP activity. A total of seven different OadB−LacZ fusions were constructed by PCR technology and used to obtain complementary evidence for the folding of OadB within the membrane by measuring β-galactosidase activities.

Alkaline Phosphatase (AP) and β-Galactosidase Activities of OadB−*PhoA and OadB*−*LacZ Fusion Products.* The AP activities of the fusion proteins, listed in Table 1, vary over the range of 0−93 Miller units. Colonies with AP activities above 5 units were blue, while those with activities below 5 units were white. Candidates of the first category were therefore regarded as positive and those of the second category as negative PhoA fusions. In-frame PhoA fusions to the cytoplasmic domain of the protein exhibit 20−40 times less activity than fusions at periplasmic domain sites (*38*). In previous topology analyses for melibiose permease (*22*) or Mtr permease (*39*) of *E. coli*, the AP activities of fusion proteins varied between 1 and 137 Miller units. The authors defined activities below 20 units as negative, between 20 and 60 units as intermediate, and above 60 units as positive.

The β-galactosidase activities of the fusion proteins, listed in Table 2, vary over the range of 0−463 Miller units. LacZ fusion proteins with activities below 50 Miller units were regarded as negative and fusions with activities above 350

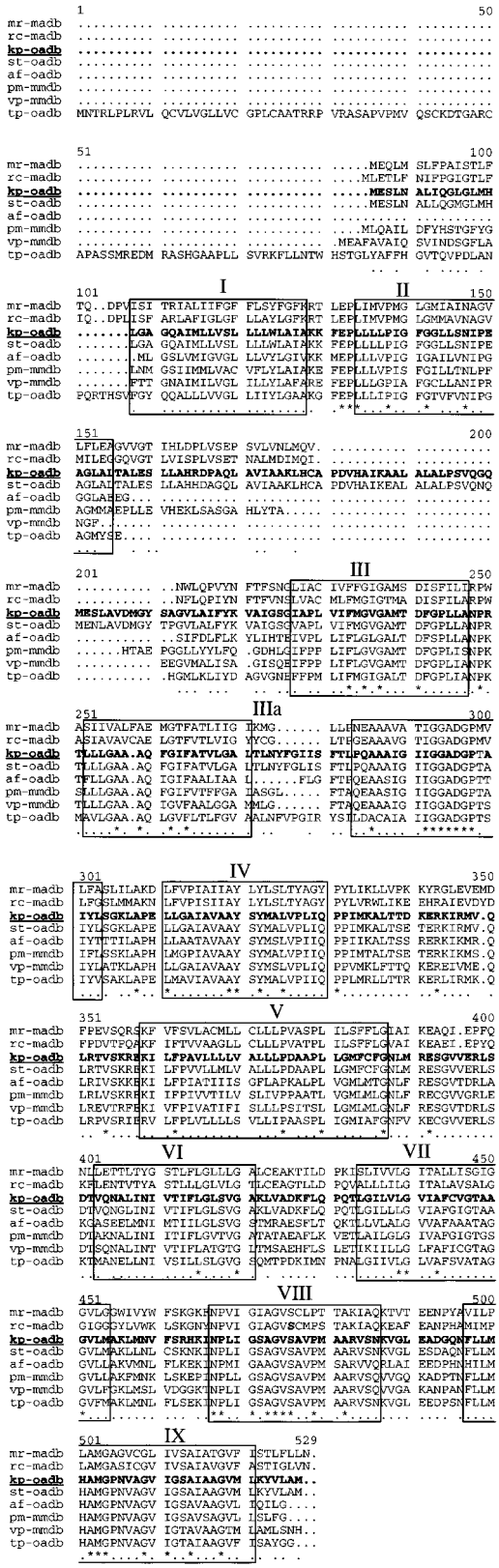

FIGURE 3: Sequence alignment of Mr-MadB with Rc-MadB (related subunit from *R. capsulatus*), Kp-OadB, St-OadB (related subunit from *Salmonella typhimurium*), Af-OadB (related subunit from *A. fulgidus*), Pm-MmdB, Vp-MmdB, and Tp-OadB (related subunit from *T. pallidum*) (for other abbrevations, see the legend of Figure 2). The putative membrane domains are boxed and numbered as described in legend of Figure 6B. Identical residues are represented by an asterisk and conservative exchanges by a dot. The sequence of Kp-OadB is bold and underlined.

Table 1: Properties of OadB−PhoA Fusion Proteins

fusion position[a]	alkaline phosphatase activity[b]	anticipated location[c]	colony color[d]	signal strength in Western blots
P41	36 ± 7	loop 1 P	blue	average
P57	56 ± 2	helix II	blue	strong
H72	17 ± 1	loop 2 C	pale blue	weak
V80	63 ± 4	loop 2 C	blue	strong
P103	2 ± 1	loop 2 C	white	strong
G134	0	loop 2 C	white	weak
N156	9 ± 2	loop 3 P	blue	strong
T179	93 ± 2	loop 4 P	blue	average
G184	33 ± 3	loop 4 P	blue	average
T189	21 ± 4	loop 4 P	blue	average
E217	12 ± 2	loop 5 P	blue	average
T245	5 ± 2	loop 6 C	white	average
L257	0	loop 6 C	white	unstable
L286	37 ± 3	helix V	blue	weak
M289	39 ± 4	helix V	blue	average
V301	10 ± 1	loop 7 P	blue	average
L329	2 ± 0	loop 8 C	white	average
Q338	3 ± 2	loop 8 C	pale blue	average
V344	11 ± 3	helix VII	blue	weak
G357	30 ± 4	helix VII	blue	unstable
V358	30 ± 7	helix VII	blue	unstable
N365	46 ± 15	loop 9 P	blue	average
A398	2 ± 0	loop 10 C	white	weak
M433	7 ± 3	C-terminus	blue	weak

[a] Amino acid in OadB after which alkaline phosphatase is fused. [b] Units of alkaline phosphatase activity calculated according to the methods of Miller (*21*) and Pourcher et al. (*22*). [c] According to the new model (Figure 6B). [d] Color of colonies of *E. coli* CC118 on $LB_{Amp100-XP40}$ plates.

Table 2: Properties of OadB−LacZ Fusion Proteins

fusion position[a]	β-galactosidase activity[b]	anticipated location[c]	signal strength in Western blots
H72	463 ± 21	loop 2 C	strong
V80	399 ± 3	loop 2 C	strong
Q167	436 ± 56	region IIIa	strong
L180	15 ± 1	loop 4 P	average
G184	0	loop 4 P	average
T189	0	loop 4 P	average
M433	29 ± 23	C-terminus	strong

[a] Amino acid in OadB after which β-galactosidase is fused. [b] Units of β-galactosidase activity calculated according to the method of Miller (*21*). [c] According to the new model (Figure 6B).

Miller units as positive. Sarsero and Pittard (*39*) found activities between 6 and 246 Miller units and distributed them into categories below 20, between 20 and 60, and above 60 Miller units. In the topological models of OadB (Figure 6), we have marked fusion sites yielding positive AP with yellow circles and those yielding negative AP with white circles. Positive LacZ fusions are shown in green circles, and negative LacZ fusions are shown in red circles.

In the following, we will go through the models by describing the results of the fusion analyses, starting from the C-terminus. In our new model (Figure 6B), we place the C-terminal methionine on the periplasmic surface, which contrasts with the model proposed previously (*27*; Figure 6A). The PhoA fusion at this side was considered positive by the blue colony color and the alkaline phosphatase activity of 7 Miller units. This comparatively low activity can be explained only by weak expression of the fusion construct (Table 1). The complementary LacZ fusion was negative with 29 Miller units, according to our definition, especially as

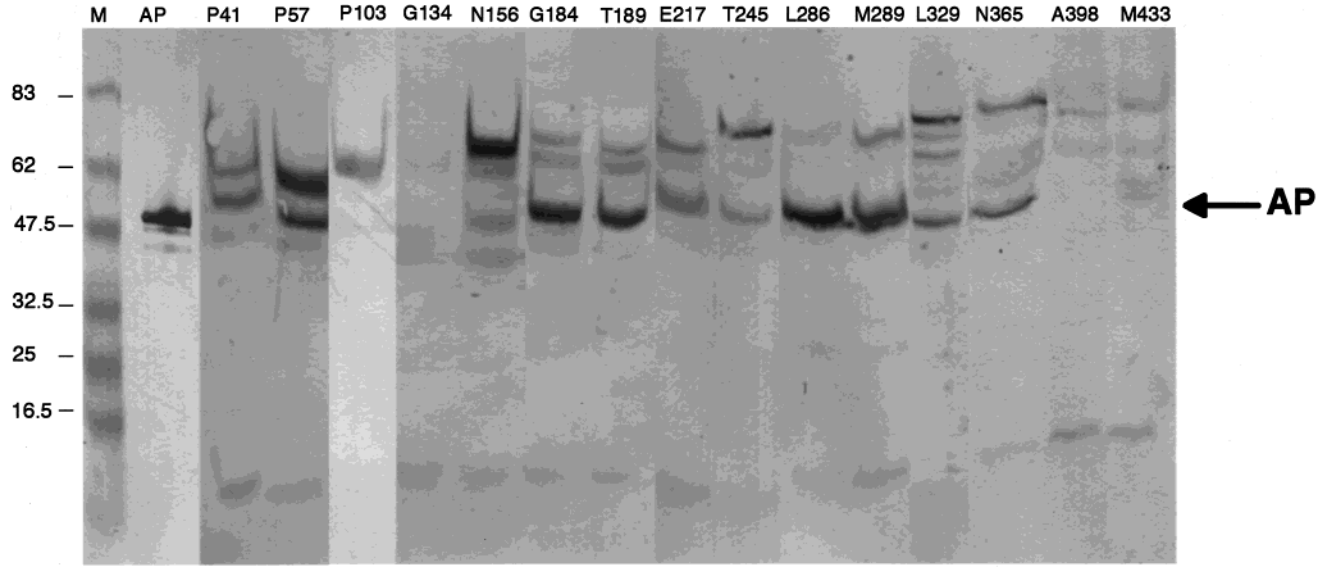

FIGURE 4: Immunoblot analysis of OadB−PhoA fusion products. Lysates of logarithmically grown cells were electrophoresed on an 8% SDS−polyacrylamide gel and blotted onto a nitrocellulose membrane. Anti-PhoA antiserum was used to detect OadB−PhoA fusion proteins. The lanes are labeled after the amino acid residue of the β-subunit, to which PhoA had been fused. Lane M shows molecular mass markers; lane AP shows purified alkaline phosphatase from *E. coli*, marked with an arrow. The upper band in the immunoblot represents the OadB−PhoA fusion protein. Bands between AP and the fusion proteins represent degradation products. Lanes M, P41, P57, G134, N156, G184, and T189 resulted from trial A, lanes AP and P103 from trial B, lanes E217 and T245 from trial C, lanes L286, M289, and L329 from trial D, lane N365 from trial E, and lanes A398 and M433 from trial F.

the fusion protein was strongly expressed. It will be shown below that an engineered cysteine at position 430, three residues before the C-terminus, was specifically accessible from the periplasm. Hence, the C-terminus is located at the periplasmic side of the membrane. This defines the orientation of helix IX, which is further supported by the low AP activity (2 Miller units, white colonies) of the A398-fused product. The membrane topology between residues 360 and 217 is the same in the two different models and therefore consistent with the results from hydropathy profiles and fusion analyses. As both N365 and the C-terminus are periplasmically located, whereas A398 faces the cytoplasm, we need to define an additional membrane-spanning helix (VIII, in Figure 6B) within the region between N365 and A398.

The information about the membrane topology of OadB obtained from the phoA and LacZ fusion approach was also valuable for the N-terminal part of the molecule, although the results were not as clear as for the C-terminal part. The positive PhoA fusions at positions 41 and 156 might indicate that these residues are in periplasmic loops, as drawn in the model shown in Figure 6B. This would indicate three transmembrane helices in the N-terminal region before N156 and a cytoplasmic location of the N-terminus. The outgoing helix I is very hydrophobic and is followed by a short hydrophilic loop and the ingoing membrane helix II (not predicted in the previous model). The polypeptide chain continues with the extended cytoplasmic loop 2 and the outgoing helix III, running from I135 to A155. The orientation of the latter helix is the same in both models and is supported by the negative PhoA fusions at P103 and G134. The two very strong LacZ fusions at H72 and V80 further support the topology of OadB, shown in Figure 6B. However, the PhoA fusions at P57, H72, and V80 were also positive and therefore apparently contradict the proposed topology. These results indicate that the short N-terminal peptides probably do not adopt unequivocal topologies, but may flip between both surfaces. Therefore, the topology cannot be predicted for the N-terminal part of the protein by fusion alone. To further analyze the topology, the location of C87 and the mutants βC87A/L7C and βC87A/V129C was determined. The cytoplasmic location of all three cysteine residues confirms the topology model depicted in Figure 6B (see below).

The hydrophobic region, flanked by residues T159 and S211, linking the N-terminal block of three membrane helices and the C-terminal block of six helices, could fold into two additional membrane-spanning segments, connected by a short loop, as proposed previously (Figure 6A). However, three positive PhoA fusions (T179, G184, and T189) and three negative LacZ fusions (L180, G184, and T189) in the suggested cytoplasmic loop do not support this model, and rather indicate that the region around residues T179−T189 is exposed to the periplasm.

Stability of Fusion Proteins. To determine whether the results obtained from the AP and β-galactosidase activity measurements correlated with the synthesis of the fusion proteins, Western immunoblot analyses of the OadB−PhoA and OadB−LacZ fusions were performed. Figure 4 shows a selection of immunoblots with OadB−PhoA fusions for which cell lysates were used. In most cases, the expected fusion products are visible, although they are accompanied by a degradation product that corresponds to the native AP and in part by additional degradation products. The approximate intensities of all OadB−PhoA fusion bands are compiled in Table 1 and of the OadB−LacZ fusion bands in Table 2. In accord with previous studies, the alkaline phosphatase fusions to periplasmic loops were usually more stable, yielding bands that were stronger than those to cytoplasmic loops or to amino acids within helices (*40*−*43*). Exceptions are the fusions at V80 and P103 within loop 2, which yielded strong signals on the immunoblot. The variance of alkaline phosphatase activities is therefore partly due to the different stabilities of the fusion products.

Table 3: Features of Cysteine Variants of OadB

OadB cysteine variant	specific activity (units/mg)	sideness[a]	anticipated location[b]
wild-type (C87)	26	cytoplasm	loop 2 C
C87A	32	not accessible	
C87A/L7C	inactive	cytoplasm	N-terminal tail
C87A/V129C	60	cytoplasm	loop 2 C
C87A/L178C	15	not accessible	region IIIa
C87A/Y182C	33	not accessible	loop 4 P
C87A/S187C	27	periplasm	loop 4 P
C87A/P191C	inactive	not accessible	region IIIa
C87A/A194C	28	not accessible	region IIIa
C87A/I198C	25	not accessible	region IIIa
C87A/P205C	0.7	not accessible	region IIIa
C87A/V430C	29	periplasm	C-terminal tail

[a] Probed with the membrane-impermeant agent IASD (*26*). [b] According to the new model (Figure 6B).

However, as alkaline phosphatase cleaved from the fusion sites may contribute to the measured AP activities, we did not attempt to correct these activities for the different levels of expression of the fusion products, as observed by the Western analyses. Nevertheless, the correlation of white colonies with very low to zero AP activities and of blue colonies with middle to high AP activities allows us with reasonable confidence to place the OadB−PhoA fusion to the cytoplasmic or periplasmic side of the membrane.

Construction of OadB Cysteine Variants and Sideness of Cysteine Residues. To construct cysteine OadB variants, we first removed the cytoplasmic cysteine 87 and changed it to an alanine. This mutation did not interfere with catalytic activity (Table 3). Membrane-located cysteines 291 and 351 did not have to be removed, because they were not accessible for IASD. Ten new OadB cysteine variants were obtained, which are listed in Table 3 together with the specific oxaloacetate decarboxylase activity, their sideness, and their anticipated location of each. All double mutants exhibited specific oxaloacetate decarboxylase activities between 15 and 60 units/mg protein, except for cysteine mutants in the N-terminal tail and for two proline mutants in the hydrophobic region IIIa, which were inactive. All mutant proteins were synthesized at levels nearly identical to that of the wild-type enzyme, except for the mutants with P/C substitutions and the cysteine mutant in the N-terminal tail, which were only poorly synthesized. Accessibility of cysteine residues was determined with the membrane-impermeable, thiol-specific fluorescent probe IASD (*26*). Labeling of periplasmically oriented cysteines was achieved by direct exposure of intact cells to the probe, while labeling of cytoplasmically oriented cysteines was performed with inside-out membrane vesicles, after external targets had been alkylated by a nonfluorescent membrane-impermeable blocking agent (MTSET). After the labeling reaction, the mutant oxaloacetate decarboxylases were purified by affinity chromatography on avidin−Sepharose, subjected to SDS−PAGE, and inspected for protein bands, containing the fluorescent label. The data depicted in Figure 5A show that the α-subunit of all decarboxylase variants that were investigated was specifically labeled from the cytoplasmic side of the membrane. In all samples, the intensities of the fluorescence of the α-subunit were comparable, as were the intensities of the silver-stained bands of the α- and β-subunits (Figure 5B). An exception is the βC87A/L7C variant, where less protein was applied to the gel. The data further show that βC87 of the wild type was exposed to the cytoplasm. Cysteine variants which became labeled from the cytoplasmic surface were βC87A/L7C and βC87A/V129C. The βC87A/L7C mutant deserves attention, because the oxaloacetate decarboxylase containing the βL7C substitution was inactive. Similar results were obtained with another cysteine mutant near the N-terminus (βC87A/L4C) and after insertion of the FLAG epitope after position M1 of the protein. Hence, an unmodified N-terminal region of OadB seems to be critical for the function of the enzyme, and therefore, the mutants in this region do not provide reliable information for assessment of the topology. A periplasmic location was on the other hand found for cysteine variants βC87A/S187C and βC87A/V430C. These results confirm exposure of the segment of region IIIa around S187 to the periplasm and further strengthen the periplasmic exposure of the C-terminal tail. The other cysteine mutants that were investigated were not labeled with the fluorescent probe applied from either side of the membrane, indicating that residues L178, Y182, P191, A194, I198, and P205 are located within the membrane or buried within a pocket of the protein. This also applies to the inaccessible cysteine residues of wild-type β-subunit residues C291 and C351.

DISCUSSION

We report here on a new model for the membrane topology of OadB (Figure 6B), which differs in several important aspects from a previous one (*27*; Figure 6A), which was based on predictions from hydropathy plots only. The hydropathy plots of OadB indicate 8−11 different hydrophobic segments with sufficient extension to span the membrane (Figure 2), and nine of these were predicted to be the only membrane-spanning domains of the previous model. Two less pronounced hydrophobic areas of OadB can be identified, following the first and preceding the last membrane domain of the previous model. Hydropathy profile alignments indicate that the area following TM helix I is clearly more hydrophobic in several related proteins, e.g., MadB, because E59 leading to a depression of hydrophobicity in OadB is replaced by V in MadB (*30*). In all related proteins, the hydrophobicity of the segment preceding the last membrane domain is clearly lower than those of the other segments, in this case being caused by a conserved arginine or lysine residue. This segment comprises the most highly conserved region of the protein besides that part of the hydrophobic segment IIIa that includes the catalytically essential D203 residue (*9*). It has therefore already been speculated that the area preceding the C-terminal helix might also have an integral membrane location (*28*).

In the following discussion, we want to go through the protein from the N-terminus to the C-terminus, describing the evidence from the various techniques used in this study for the folding of OadB within the membrane. OadB has a blocked N-terminal methionine, which was defined by sequencing of the appropriate cyanogen bromide peptide (*2*). We propose in our new model (Figure 6B) that a tail of approximately 15 N-terminal amino acids is exposed to the cytoplasm. OadB with an L7C mutation was specifically alkylated from the cytoplasmic side of the membrane. Unfortunately, the above-mentioned mutant did not exhibit oxaloacetate decarboxylase activity and, therefore, does not provide valuable information for assessment of the topology.

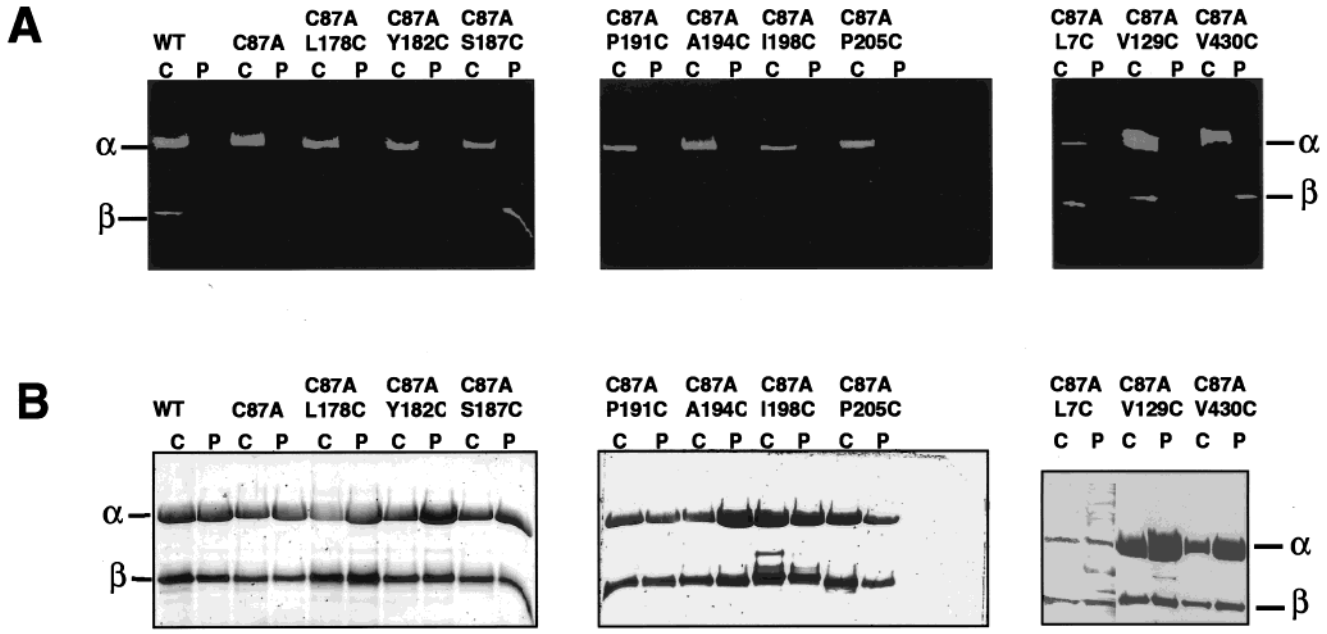

FIGURE 5: SDS−PAGE of purified oxaloacetate decarboxylases after site-specific labeling of cysteine residues with the fluorescent probe IASD and corresponding silver-stained SDS gels. (A) Cysteine residues accessible from the periplasm (P) and cytoplasm (C) and (B) corresponding silver-stained SDS gels. The soluble α-subunit serves as a positive control for accessibility from the cytoplasm, as it contains four cysteine residues. Wild type and cysteine variants βC87A, βC87A/L178C, βC87A/Y182C, βC87A/S187C, βC87A/P191C, βC87A/A194C, βC87A/I198C, βC87A/P205C resulted from trial A, βC87A/L7C from trial B, and βC87A/V129C and βC87A/V430C from trial C. Twenty micrograms of protein was applied per sample, except for the βC87A/L7C variant, where 6.8 μg of protein was applied.

This phenotype was also observed with another cysteine mutant (βC87A/L4C) or by inserting a FLAG epitope into the N-terminal tail. Therefore, this part of the molecule seems to be critical for the functional integrity of the decarboxylase. Such a critical role would be more consistent with an internal location, perhaps at the interface with the α-subunit, rather than an external (periplasmic) location.

The first TM helix (I) is very hydrophobic and runs from L16 to A36. This is followed by the first periplasmic loop, comprising amino acids $K_{37}KFEP_{41}$ and the less hydrophobic helix II, which runs from L42 to L63. The positive PhoA fusion at position P41 within the periplasmic loop is in accord with this folding. However, a positive PhoA fusion at P57 within helix II and fusions at H72 and V80 in the adjacent cytoplasmic loop indicate that within this short N-terminal region of OadB the PhoA fusion technique fails to make reliable predictions about the topology. Anomalously high levels of alkaline phosphatase activity near the N-terminus of cytoplasmic loops of membrane proteins is a well-recognized phenomenon (*44*). Therefore, the topology of this area has also been analyzed by LacZ fusions at H72 and V80, and both had very high β-galactosidase activities. The cytoplasmic location of the extended loop connecting helices II and III was supported by the negative PhoA fusions at P103 and G134 in the C-terminal part of this loop. Furthermore, the wild-type cysteine 87 and cysteine replacing valine at position 129 were both exclusively alkylated from the cytoplasm. It should also be noted that the extended cytoplasmic loop 2 is a specific property of OadB from *K. pneumoniae* and *S. typhimurium*, whereas the related β-subunit of methylmalonyl-CoA decarboxylase of *V. parvula* has only 15 amino acid residues in this region with no apparent similarity to its relatives. Hence, folding of the OadB region between amino acids 64 and 134 into an additional TM helix is unlikely. The next TM helix runs from I135 to A155 and is defined by the results just mentioned and the AP-positive fusion at N156.

Following the short peptide $N_{156}PRT_{159}$, which includes a conserved proline residue, the OadB sequence continues with a hydrophobic region between L160 and L210 that has been termed region IIIa. The topology analysis of this area yielded a positive LacZ fusion at Q167, positive PhoA fusions at T179, G184, and T189, and negative LacZ fusions at L180, G184, and T189. In addition, S187 has been mutagenized into a cysteine residue, and this was shown to be periplasmically exposed. A cysteine introduced at position 182 was not accessible to the alkylaing probe and may therefore have an integral membrane location or may be buried within a pocket of the protein. These results strongly indicate that the peptide comprising T179 to T189 extends into the periplasm. On the basis of the hydrophobicity of the sequence between L160 and L178, this portion of the protein should insert into the membrane. However, it is too short to span the membrane as two α-helices. We propose, therefore, that the polypeptide chain following L160 inserts into the membrane from the periplasm and folds backward to emerge from its surface again with T179. Such very short membrane-integral α-helical structures have been identified in the pore helices of the potassium channel from *Streptomyces lividans*, whose structure was determined recently by X-ray analysis at 3.2 Å (*45*). It may be worth mentioning that defining the region between T179 and T189 as a periplasmic loop rather than as an integral membrane portion is more compatible with the gaps of five to six residues found here in the various related proteins. For the region between L190 and L210, we propose again that it inserts from the periplasm into the membrane, but not so far as to reach the cytoplasmic surface. Rather, the polypeptide chain turns the direction and emerges from the perplasmic surface with S211. The integral membrane location of this area is likely because of the inacces-

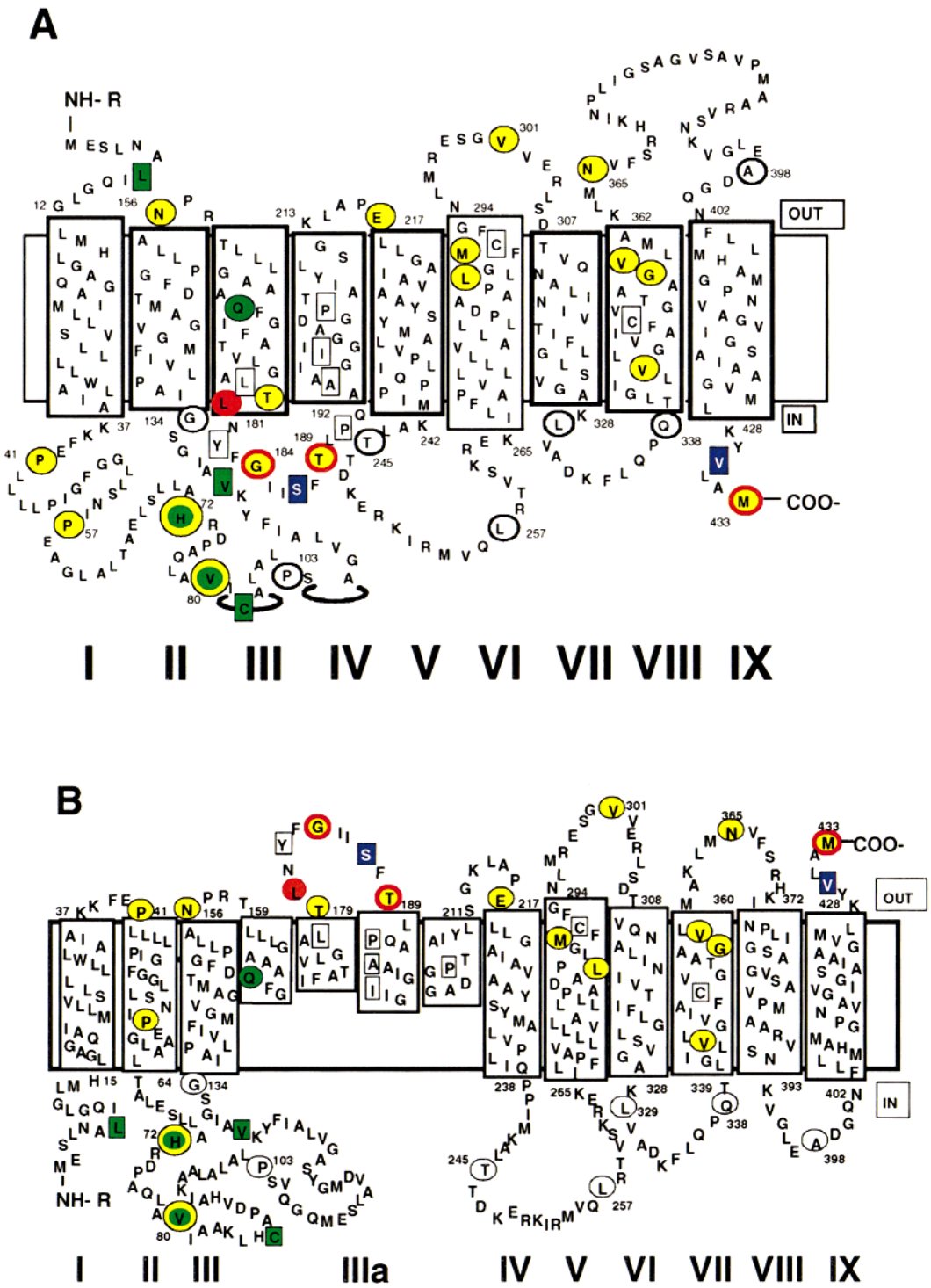

FIGURE 6: Topological models of the oxaloacetate decarboxylase β-subunit. The amino acid residues, to which the signal sequence-depleted alkaline phosphatase (AP) or β-galactosidase was fused, are marked by circles. Fusion sites yielding clones with positive AP activities (>5 units, blue colonies) are yellow, and those with negative AP activities (<5 units, white colonies) are white. Fusion sites yielding clones with positive β-galactosidase activities are green (>350 units), and those with negative β-galactosidase activities (<50 units) are red. The yellow circles outlined in red mean red and yellow circles, e.g., negative LacZ and positive PhoA fusion. The green circles outlined in yellow mean green and yellow circles, e.g., positive LacZ and positive PhoA fusion. The amino acid residues, which had been changed to cysteines, are indicated by squares. Cysteines, which are labeled from the cytoplasmic side, are green, and those which are labeled from the periplasmic side blue, and those which are not labeled from either side white. Panel A shows the previous model (*27*). Panel B shows the new model.

sibility of four cysteine mutants (βC87A/P191C, βC87A/A194C, βC87A/I198C, and βC87A/P205C) to the polar fluorescent alkylating agent IASD. The putative role of D203 as a binding site for Na^+ or H^+ during the transport of these cations across the membrane (*9*) would hardly be compatible with a location of this residue outside the membrane. The critical role of this area is further indicated by seven invariant residues around the universal and functionally indispensable D203. The enzymic activity was completely abolished even with the most conservative exchange of D203 with E (*9*). In the βC87A/P191C or βC87A/P205C mutants, the oxaloacetate decarboxylase activity was either severely reduced or

extinguished. Likewise, the insertion of FLAG epitopes (DYKDDDK) between amino acids L178 and Y182 led to inactive oxaloacetate decarboxylases. Hence, several mutations in this part of the molecule have drastic effects on the catalytic activity of the enzyme, corroborating its functional significance.

It is envisaged that the polypeptide emerges from the membrane again with the periplasmic peptide S_{211}GKLAPE$_{217}$. The next TM helix (IV) runs from L218 to Q237 and is continued as a highly charged cytoplasmic loop between P238 and K265. This folding is in accord with the positive PhoA fusion at E217 and two negative PhoA fusions at T245 and L257. The protein curls again into a TM helix (V) between I266 and G293 and forms the periplasmic loop between N294 and T308. The folding is supported by three positive PhoA fusions at L286, M289, and V301 and the inaccessibility of C291 to the charged alkylating agent IASD. The next TM helix (VI) starts with V309 and ends with A327. The following cytoplasmic loop is supported by the two negative PhoA fusions at L329 and Q338. As pale blue colonies were obtained at the latter fusion site, Q338 may alternatively be located within the next outgoing TM helix (VII), which could start with F334 already. Within this helix and the adjacent periplasmic loop, positive PhoA fusions were obtained at V344, G357, V358, and N365. The positive PhoA fusions within the helix are in accord with the notion that five or more residues of an outgoing TM helix could promote the export of AP (*40*, *46*). The folding of OadB in the region comprising TM helices IV−VII is the same in the previous model and our model presented here. The old model predicted a large periplasmic loop and an ingoing TM helix for the C-terminal part of the molecule. This folding, however, is not in accord with a negative PhoA fusion at A398 and the positive PhoA and negative LacZ fusion at the C-terminal methionine. Furthermore, cysteine introduced at position 430 instead of valine within the C-terminal tail was specifically alkylated by IASD from the periplasmic surface. Hence, the periplasmic loop is shorter than was assumed previously, and the highly conserved segment, flanked by I372 and K393, forms another TM helix (VIII). This is followed by the cytoplasmic loop between K393 and N402 and the outgoing TM helix IX, placing the C-terminus into the periplasm.

In summary, the new topology of OadB described here predicts two additional TM helices (II and VIII) with respect to the previous one and also places the N-terminus in the cytoplasm and the C-terminus in the periplasm, the opposite of their orientation proposed previously. In addition, the previously predicted fold of the region between amino acids 159 and 211 into two membrane-spanning helices and a cytoplasmic loop could not be confirmed. This region is now thought to fold into two pairs of membrane-inserted segments, which are connected by a periplasmic loop.

One of the criterion for predicting the orientation of helices within the membrane is the "positive-inside-rule", introduced by von Heijne (*47*). With regard to the topology of OadB, there appear to be major exceptions. The cytoplasmic N-terminus carries a negative charge; the first, third, and ninth periplasmic loops are positively charged, and the charges in the second large cytoplasmic loop are essentially balanced. The rule clearly applies to the sixth cytoplasmic loop, which is the most hydrophilic part of the molecule and contains nine positively charged R and K residues and two negatively charged D and E residues. The rule is valid also for cytoplasmic loop 8, which contains two K residues and one D residue. However, cytoplasmic loop 10 contains one positive and two negative charges, and periplasmic loop 9 has three positively charged and no negatively charged amino acids. It is possible, therefore, that the main determinant for the proper insertion of OadB into the membrane is the highly positively charged cytoplasmic loop 6. Overall, OadB has a net charge of +4 in the cytoplasmic loops and a net charge of +4 in periplasmic loops.

We provide here with confidence information about the folding of the oxaloacetate decarboxylase β-subunit within the membrane. This topology is a suitable point of departure for functional studies of the Na^+ pump by site-directed mutagenesis. We will report elsewhere that specific mutations within the newly recognized helix VIII abolish the oxaloacetate decarboxylase activity, thus emphasizing the functional significance of amino acids in this region.

ACKNOWLEDGMENT

We are grateful to Dr. L. Hederstedt (Department of Microbiology, University of Lund, Lund, Sweden) for providing the polyclonal AP antibody. Kathryn Adcock and Günther Woehlke did preliminary work in constructing PhoA−OadB fusion proteins.

SUPPORTING INFORMATION AVAILABLE

Table A listing the primers used for generation of *oadB−'phoA* fusions and *oadB−'lacZ* fusions and Table B listing the primers used for construction of site-specific cysteine mutants in OadB. This material is available free of charge via the Internet at http://pbs.acs.org.

REFERENCES

1. Woehlke, G., Laussermair, E., Schwarz, E., Oesterhelt, D., Reinke, H., Beyreuther, K., and Dimroth, P. (1992) *J. Biol. Chem. 267*, 22804−22805.
2. Laussermair, E., Schwarz, E., Oesterhelt, D., Reinke, H., Beyreuther, K., and Dimroth, P. (1989) *J. Biol. Chem. 264*, 14710−14715.
3. Schwarz, E., Oesterhelt, D., Reinke, H., Beyreuther, K., and Dimroth, P. (1988) *J. Biol. Chem. 263*, 9640−9645.
4. Dimroth, P. (1997) *Biochim. Biophys. Acta 1318*, 11−51.
5. Dimroth, P., and Schink, B. (1998) *Arch. Microbiol. 170*, 69−77.
6. Di Berardino, M., and Dimroth, P. (1995) *Eur. J. Biochem. 231*, 790−801.
7. Dimroth, P., and Thomer, A. (1983) *Eur. J. Biochem. 137*, 107−112.
8. Dimroth, P., and Thomer, A. (1988) *Eur. J. Biochem. 175*, 175−180.
9. Di Berardino, M., and Dimroth, P. (1996) *EMBO J. 15*, 1842−1849.
10. Bott, M., and Dimroth, P. (1994) *Mol. Microbiol. 14*, 347−356.
11. Dimroth, P., and Thomer, A. (1992) *FEBS Lett. 300*, 67−70.
12. Braune, A., Bendrat, K., Rospert, S., and Buckel, W. (1999) *Mol. Microbiol. 31*, 463−472.
13. Hilpert, W., and Dimroth, P. (1983) *Eur. J. Biochem. 132*, 579−587.
14. Yanish-Perron, C., Vieira, J., and Messing, J. (1995) *Gene 33*, 103−119.
15. Manoil, C., and Beckwith, J. (1985) *Proc. Natl. Acad. Sci. U.S.A. 82*, 8129−8133.

16. Sambrook, J., Fritsch, E. F., and Maniatis, T. (1989) in *Molecular cloning: A laboratory manual*, 2nd ed., Cold Spring Harbor Laboratory Press, Cold Spring Harbor, NY.
17. Sanger, F., Nicklen, S., and Coulson, A. R. (1977) *Proc. Natl. Acad. Sci. U.S.A. 74*, 5463−5467.
18. Hoffman, C. S., and Wright, A. (1985) *Proc. Natl. Acad. Sci. U.S.A. 82*, 5107−5111.
19. Henikoff, S. (1984) *Gene 28*, 351−359.
20. Minton, N. P. (1984) *Gene 31*, 269−273.
21. Miller, J. H. (1972) in *Experiments in molecular genetics*, Cold Spring Harbor Laboratory Press, Cold Spring Harbor, NY.
22. Pourcher, T., Bibi, E., Kaback, H. R., and Leblanc, G. (1996) *Biochemistry 35*, 4161−4168.
23. Dimroth, P. (1986) *Methods Enzymol. 125*, 530−540.
24. Schägger, H., and von Jagow, G. (1987) *Anal. Biochem. 166*, 368−379.
25. Hofmann, K., and Stoffel, W. (1993) *Biol. Chem. Hoppe-Seyler 347*, 166.
26. Fu, D. X., and Maloney, P. C. (1998) *J. Biol. Chem. 273*, 17962−17967.
27. Woehlke, G., Wifling, K., and Dimroth, P. (1992) *J. Biol. Chem. 267*, 22798−22803.
28. Huder, B. J., and Dimroth, P. (1993) *J. Biol. Chem. 268*, 24564−24571.
29. Bott, M., Pfister, K., Burda, P., Kalbermatter, O., Woehlke, G., and Dimroth, P. (1997) *Eur. J. Biochem. 250*, 590−599.
30. Berg, M., Hilbi, H., and Dimroth, P. (1997) *Eur. J. Biochem. 245*, 103−115.
31. Klenk, H. P., Clayton, R. A., Tomb, J., White, O., Nelson, K. E., Ketchum, K. A., et al. (1997) *Nature 390*, 364−370.
32. Fraser, C. M., Norris, S. J., Weinstock, G. M., White, O., Sutton, G. G., Dodson, R., et al. (1998) *Science 281*, 375−388.
33. Manoil, C. (1990) *J. Bacteriol. 172*, 1035−1042.
34. Manoil, C., Mekalanos, J. J., and Beckwith, J. **(**1990) *J. Bacteriol. 172*, 515−518.
35. Manoil, C. (1992) *Methods Cell Biol. 34*, 61−75.
36. Traxler, B., Boyd, D., and Beckwith, J. **(**1993) *J. Membr. Biol. 132*, 1−11.
37. Sugiyama, J. E., Mahmoodian, S., and Jacobson, G. R. (1991) *Proc. Natl. Acad. Sci. U.S.A. 88*, 9603−9607.
38. Manoil, C., and Beckwith, J. (1986) *Science 233*, 1403−1408.
39. Sarsero, J. P., and Pittard, A. J. (1995) *J. Bacteriol. 177*, 297−306.
40. Boyd, D., Manoil, C., and Beckwith, J. (1987) *Proc. Natl. Acad. Sci. U.S.A. 84*, 8525−8529.
41. Derman, A. I., and Beckwith, J. (1991) *J. Bacteriol. 173*, 7719−7722.
42. Derman, A. I., and Beckwith, J. (1995) *J. Bacteriol. 177*, 3764−3770.
43. San Millan, J. L., Boyd, D., Dalbey, R., Wickner, W., and Beckwith, J. **(**1989) *J. Bacteriol. 171*, 5536−5541.
44. Prinz, W. A., and Beckwith, J. (1994) *J. Bacteriol. 176*, 6410−6413.
45. Doyle, D. A., Cabral, J. M., Pfuetzner, R. A., Kuo, A., Gulbis, J. M., Cohen, S. L., Chait, B. T., and MacKinnon, R. (1998) *Science 280*, 69−76.
46. Calamia, J., and Manoil, C. (1990) *Proc. Natl. Acad. Sci. U.S.A. 87*, 4937−4941.
47. von Heijne, G. (1992) *J. Mol. Biol. 225*, 487−494.

BI990303+